

Figure S1



● Bay ○ Wind station

Figure S2

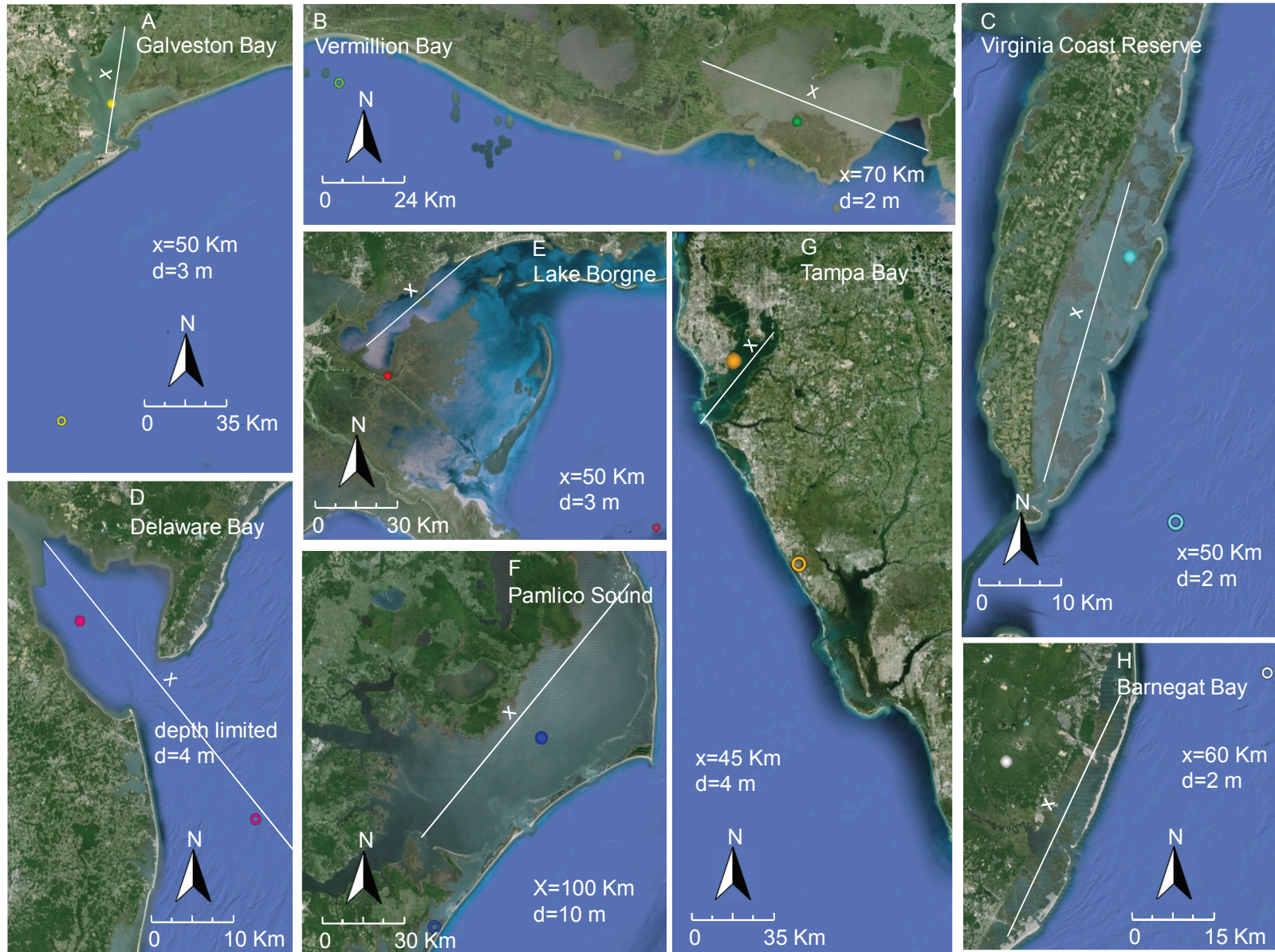


Figure S3

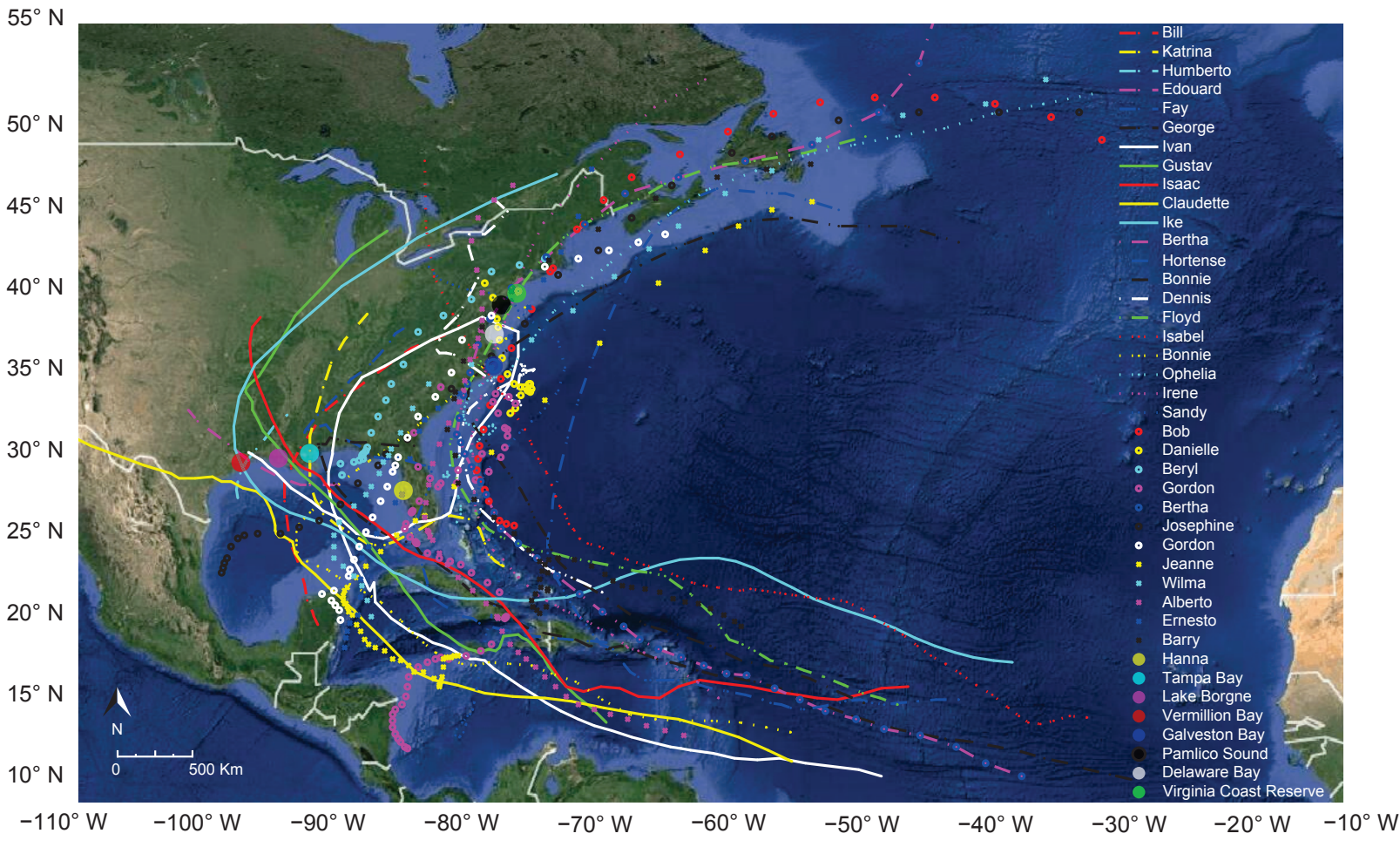


Figure S4

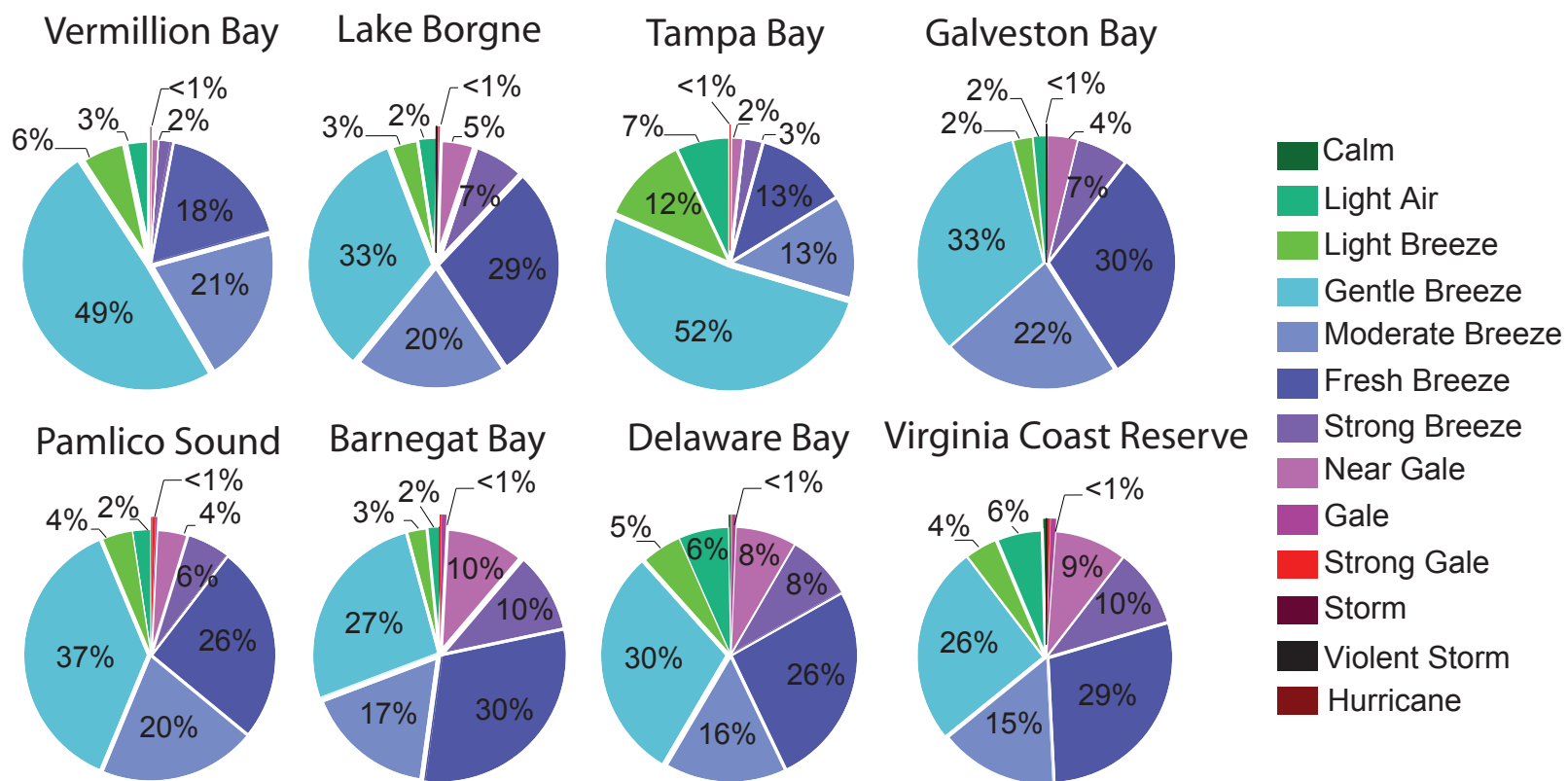


Figure S5

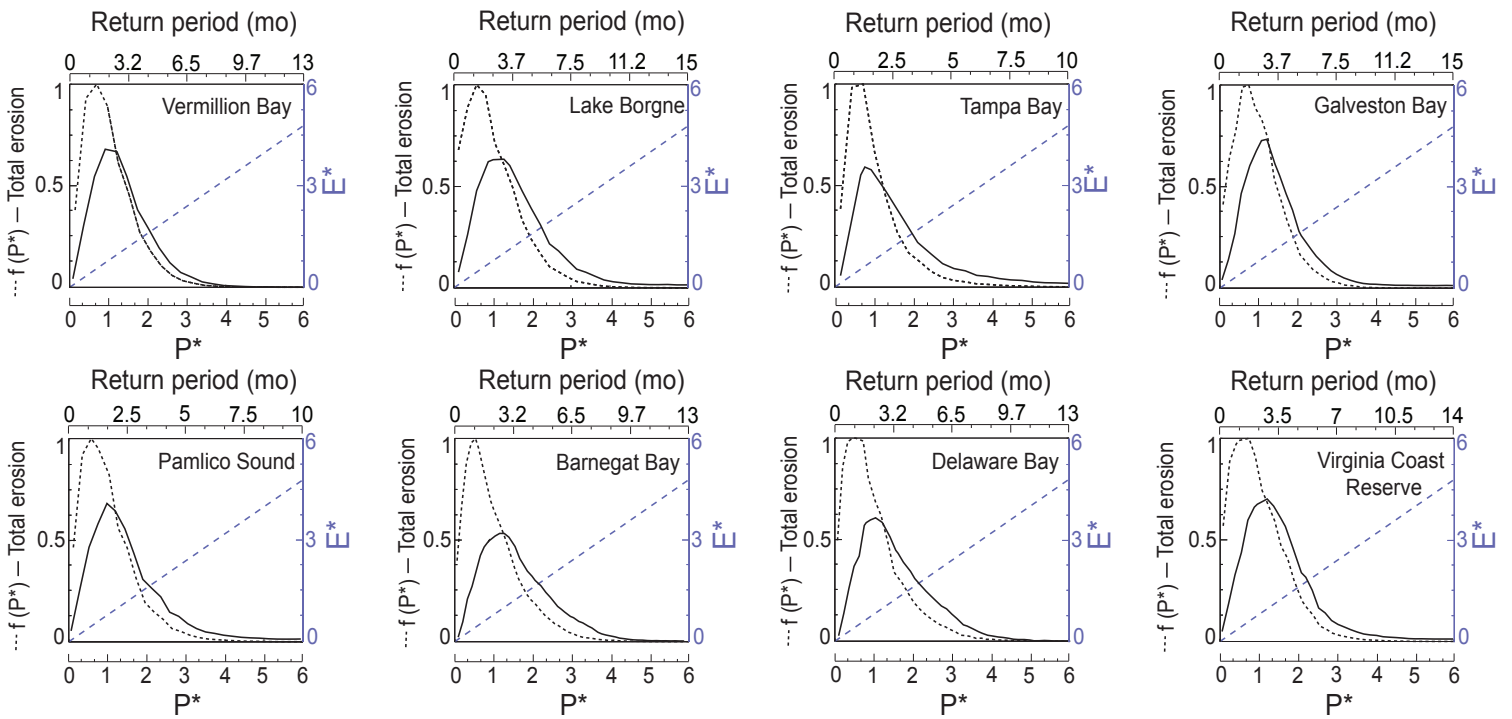


Figure S6

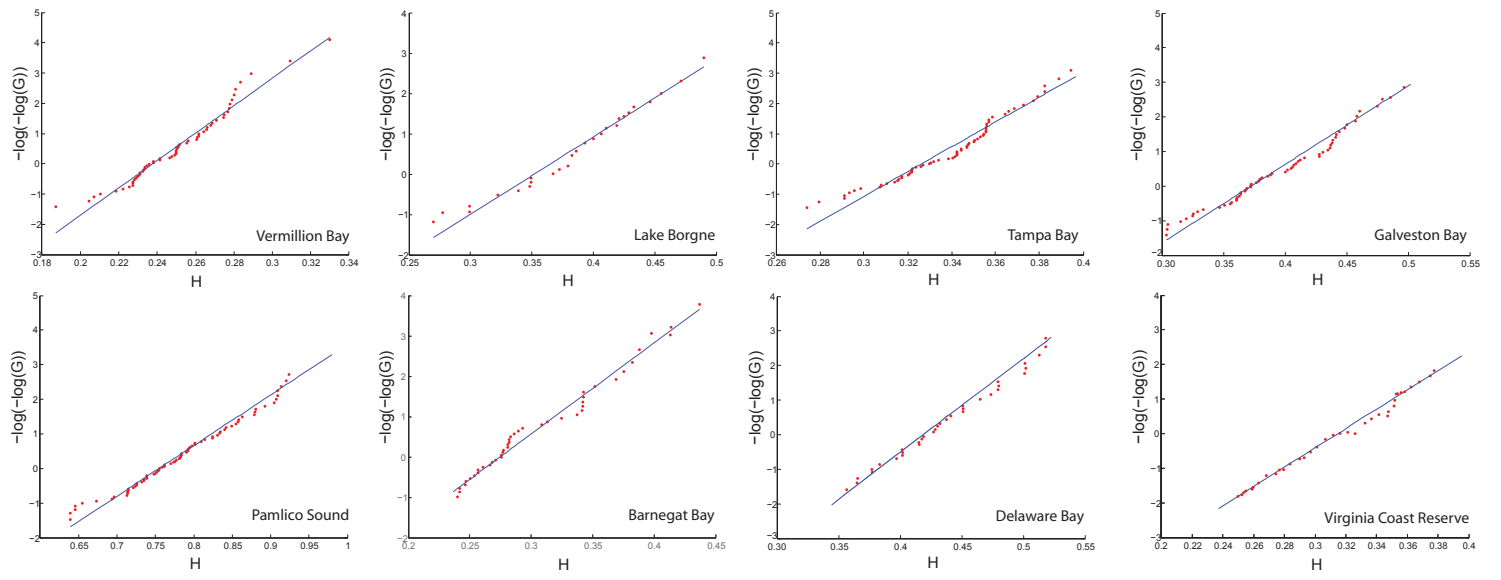


Figure S7

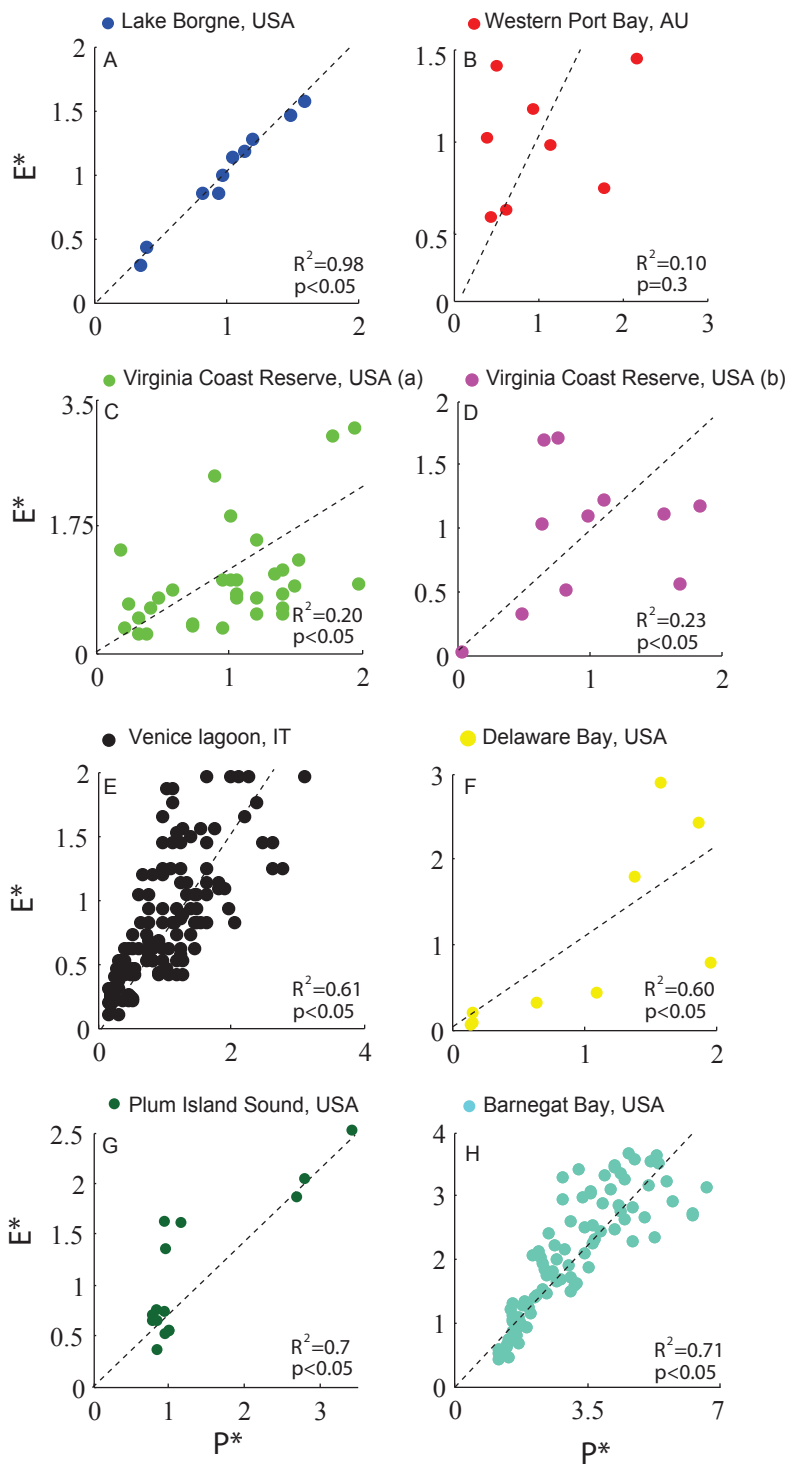


Figure S8

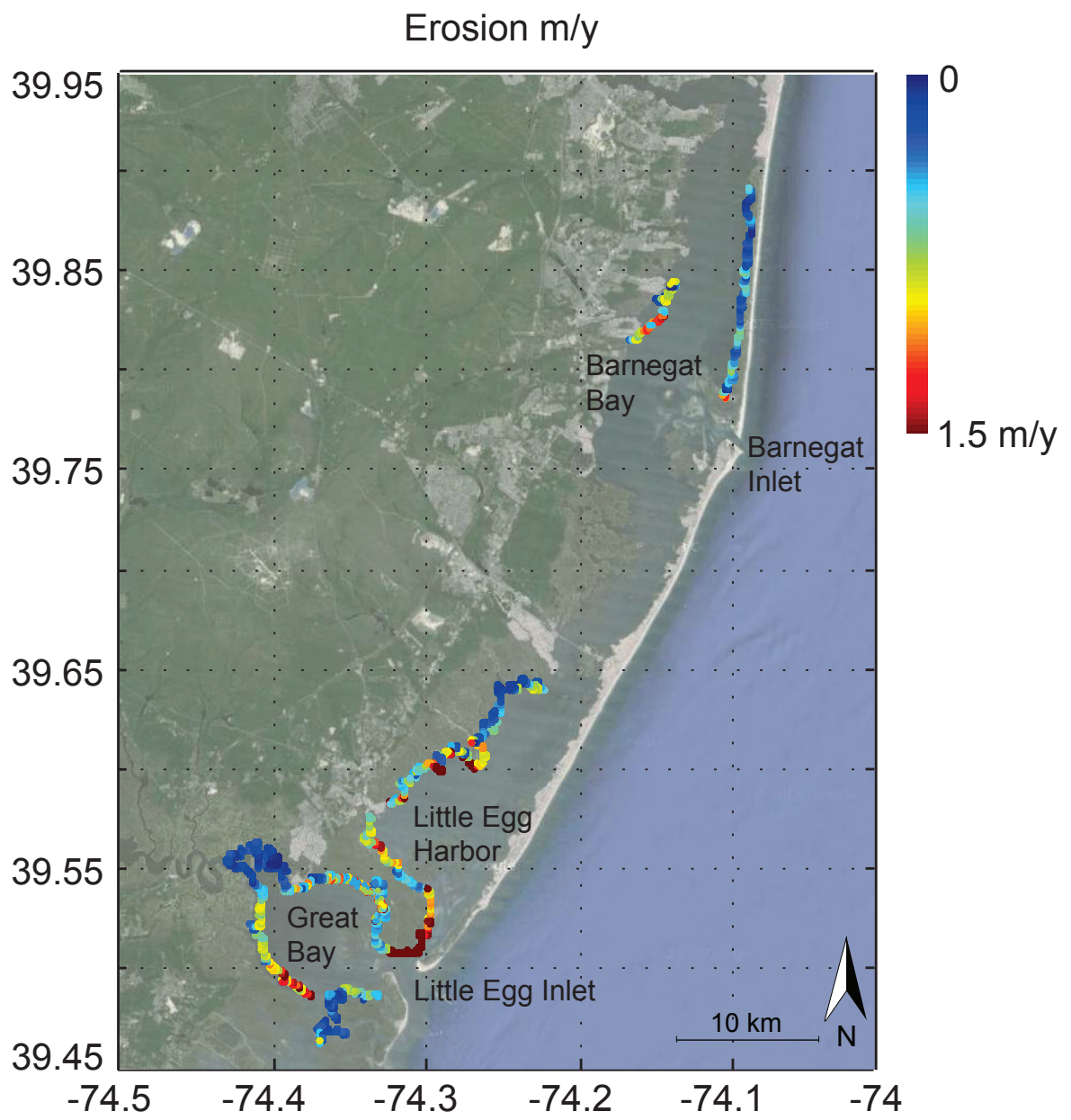


Figure S9

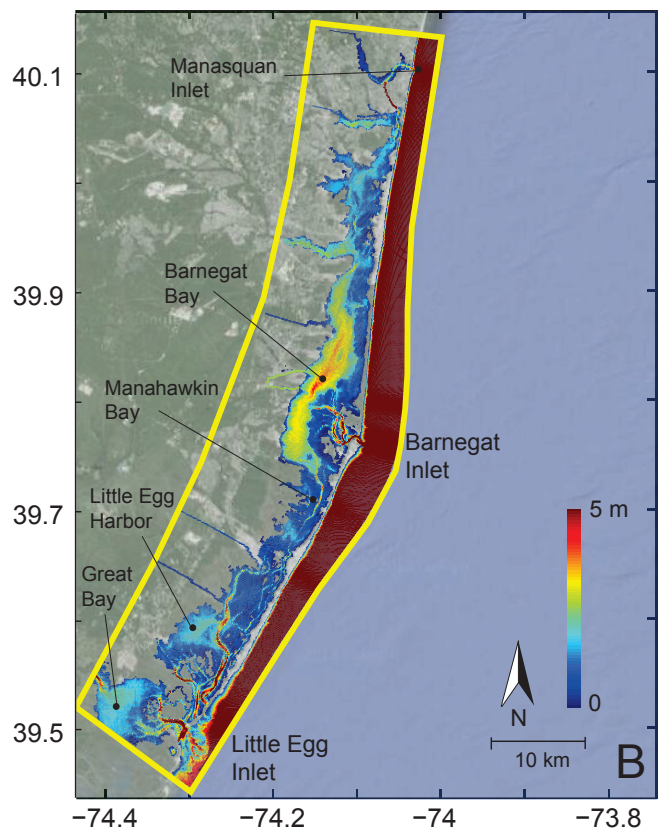
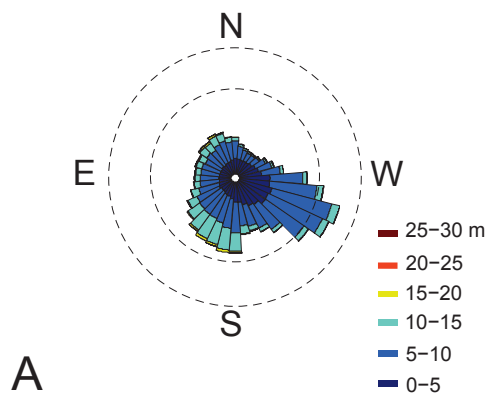


Figure S10

STORM NAME	DATE ACTIVE	STORM CATEGORY (SSHWS/NWS)
Bill	June 29-July 2, 2003	Tropical Storm
Katrina	August 23-August 31, 2005	Category 5 major hurricane
Humberto	September 12-September 14, 2007	Category 1 hurricane
Fay	August 15-August 29, 2008	Tropical Storm
Edouard	August 3-August 6, 2008	Tropical storm
George	September 15 - October 1, 1998	Category 4 major hurricane
Ivan	September 2 - September 24, 2004	Category 5 major hurricane
Gustav	August 25 - September 7, 2008	Category 4 major hurricane
Isaac	August 21 - September 3, 2012	Category 1 hurricane
Gabrielle	September 11 - September 19, 2001	Category 1 hurricane
Claudette	July 8 - July 17, 2003	Category 1 hurricane
Ike	September 1 - September 15, 2008	Category 4 major hurricane
Bertha	July 5 - July 18, 1996	Category 3 major hurricane
Horthense	September 3, September 16, 1996	Category 4 major hurricane
Bonnie	August 19, August 30, 1998	Category 3 major hurricane
Dennis	August 24 - September 7, 1999	Category 2 hurricane
Floyd	September 7 - September 19, 1999	Category 4 major hurricane
Isabel	September 6 - September 20, 2003	Category 5 major hurricane
Bonnie	August 3 - August 14, 2004	Tropical storm
Ophelia	September 6 - September 23, 2005	Category 1 hurricane
Irene	August 21 - August 30, 2011	Category 3 major hurricane
Sandy	October 22 - November 2, 2012	Category 3 major hurricane
Bob	August 16 - August 20, 1991	Category 3 major hurricane
Danielle	September 22 - September 26, 1992	Tropical storm
Beryl	August 14 - August 19, 1994	Tropical storm
Gordon	November 8 - November 23, 1994	Category 1 hurricane
Bertha	July 5 - July 18, 1996	Category 3 major hurricane
Josephine	October 4 - October 13, 1996	tropical storm
Bonnie	August 19 - August 30, 1998	Category 3 major hurricane
Dennis	August 24 - September 7, 1999	Category 2 hurricane
Floyd	September 7 - September 19, 1999	Category 4 major hurricane
Gordon	September 14 - September 21, 2000	Category 1 hurricane
Isabel	September 6 - September 20, 2003	Category 5 major hurricane
Jeanne	September 13 - September 29, 2004	Category 3 major hurricane
Wilma	October 16 - October 30, 2005	Category 5 major hurricane
Alberto	June 10 - June 14, 2006	Tropical storm
Ernesto	August 24 - September 1, 2006	Category 1 hurricane
Barry	June 1 - June 5, 2007	Tropical storm
Hanna	August 28 - September 7, 2008	Category 1 hurricane
Sandy	October 22 - November 2, 2012	Category 3 major hurricane

Table S1

Figure S1. A) Location of field measurements collected in Plum Island Sound, USA. Boundary measurements have been taken at high resolution for stretches of shoreline around 100 m long. The three locations are Refuge North ($42^{\circ}45'00$ N $70^{\circ} 48' 00$ W), Stackyard Road ($42^{\circ}44'00$ N $70^{\circ} 49' 00$ W) and Refuge South ($42^{\circ}44'00$ N $70^{\circ} 48' 00$ W). Marsh contours have been tracked using a Real-Time Kinematic-Global Positioning System (RTK-GPS) and an electronic Total Station every year from 2008 to 2013. Data were collected with an average resolution of 1 m. When marsh contours were characterized by significant variations in boundary geometry, measurements were taken up to 20 cm apart. B) Marsh boundary at Stackyard Road. Different colors are measurements at different years. The boundary presented in this plot is eroding at an average rate of 0.35 m/y. Is it possible to notice that the erosion occurred during Hurricane Sandy is negligible for great part of the shoreline, and smaller than the average yearly erosion.

Figure S2. Location of bays and wind stations used in the study for the calculation of wave power, erosion rate, and total erosion (courtesy Google Earth, see also Methods).

Figure S3. Detailed view of bays and wind stations used in the study for the calculation of wind waves and total erosion: A, Galveston Bay, Texas; B, Vermillion Bay, Louisiana; C, Virginia Coast Reserve, Virginia; D, Delaware Bay, Delaware; E, Lake Borgne, Louisiana; F, Pamlico Sound, North Carolina; G, Tampa Bay, Florida; H, Barnegat Bay, New Jersey. Maximum fetch (x , white line), and average water depths (d) are indicated as well (courtesy Google Earth).

Figure S4. Path of major hurricanes that affected the areas of interest from 1991 to 2013 (See Table S1 for storms category and date). Locations of studied bays are indicated.

Figure S5. Contribution of different wind categories to the erosion rate of each site. Plots refer to the entire period of record.

Figure S6. Frequency-magnitude distribution of dimensionless wave power, $f(P^*)$ (dashed black line), total erosion (continuous black line), dimensionless erosion rate, E^* , (dashed blue line), as a function of P^* . The return period T (months), corresponding to a given wave power, P^* , is indicated as well.

Figure S7. Frequency of wave events computed using a Gumbel distribution. On the horizontal axis wave height observations are indicated, while on the vertical axis the reduced variable $\log(-\log(G))$ is shown. The blue lines fit the data according to the Gumbel distribution (See Methods).

Figure S8. Non dimensional wave power and non-dimensional erosion rates for each individual study site. Colors used are the same of Figure 1. A) Lake Borgne, USA; B) Western Port Bay, AU; C) Virginia Coast Reserve, USA (a); D) Virginia Coast Reserve, USA (b); E) Venice Lagoon, IT; F) Delaware Bay, USA; G) Plum Island Sound; H) Barnegat Bay, USA.

Figure S9. Erosion rates (m/y) in Barnegat Bay. Erosion rates were obtained by digitalizing more than 100 km of marsh shoreline using aerial images (1930, 2007 and 2013) from the digital orthophotography of New Jersey (see also Methods). Erosion rate has been obtained by comparing images from 1930, and 2007 and from 2007 to 2013, dividing by the number of years,

and averaging between the two data-sets. Aerial images from 2012 and 2013 have been compared as well to have information about changes in marsh boundaries before and after Hurricane Sandy. However, for these two years changes in marsh boundaries could not be detected at the resolution of the given images.

Figure S10. A) Wind rose for the Barnegat Bay-Little Egg Harbor system (National Data Buoy station LLNR 830 40.251 N 73.164 W) for the period from 1991-2013. B) Bathymetry of the Barnegat-Bay Little Egg Harbor system. Yellow lines indicate the boundaries of the computational domain. The model used to calculate wind waves is the Coupled-Ocean-Atmosphere-Wave-Sediment-Transport (COAWST) Modeling System^{1,2}. In COAWST the ocean model ROMS, the atmospheric model WRF, the wave model SWAN, and the modules of the Community Sediment Transport Model are fully coupled by means of the Model Coupling Toolkit. The ocean model ROMS is a three-dimensional, free-surface, terrain-following model solving finite difference approximations of the Reynolds Averaged Navier-Stokes equations, using hydrostatic and Boussinesq assumptions^{3,4}.

The model was run for wind speed ranging from 5 to 30 m/s, and for different wind directions. Wind data (speed and direction) from 1991 to 2013 were retrieved from a nearby NOAA station (station ID LLNR 830). Wave information for each point along the marsh shoreline, corresponding to different wind directions and wind speed conditions, were used to reconstruct the long-term average wave climate in the area. See also 5, for more details about the model.

Table S1. Major hurricanes and tropical storms that have affected the areas of interest; Storm name, date, and category according to the Saffir-Simpson hurricane scale are reported. Data are available at (<http://www.weather.gov/>).

References

1. Warner, J. C., C. R. Sherwood, R. P. Signell, C. K. Harris, and H. G. Arango (2008), Development of a three-dimensional, regional, coupled wave, current, and sediment-transport model, *Computers & Geosciences*, 34(10), 1284–1306, doi:<http://dx.doi.org/10.1016/j.cageo.2008.02.012>.
2. Warner, J. C., B. Armstrong, R. He, and J. B. Zambon (2010), Development of a Coupled Ocean–Atmosphere–Wave–Sediment Transport (COAWST) Modeling System, *Ocean Modelling*, 35(3), 230–244, doi:<http://dx.doi.org/10.1016/j.ocemod.2010.07.010>.
3. Chassignet, E. P., H. Arango, D. Dietrich, T. Ezer, M. Ghil, D. B. Haidvogel, C.-C. Ma, A. Mehra, A. M. Paiva, and Z. Sirkes (2000), DAMÉE-NAB: the base experiments, *Dynamics of Atmospheres and Oceans*, 32(3–4), 155–183, doi:[http://dx.doi.org/10.1016/S0377-0265\(00\)00046-4](http://dx.doi.org/10.1016/S0377-0265(00)00046-4).
4. Shchepetkin, A. F., and J. C. McWilliams (2005), The regional oceanic modeling system (ROMS): a split-explicit, free-surface, topography-following-coordinate oceanic model, *Ocean Modelling*, 9(4), 347–404, doi:<http://dx.doi.org/10.1016/j.ocemod.2004.08.002>.
5. Defne, Z., and N. Ganju (2014), Quantifying the Residence Time and Flushing Characteristics of a Shallow, Back-Barrier Estuary: Application of Hydrodynamic and Particle Tracking Models, *Estuaries and Coasts*, 1–16, doi:10.1007/s12237-014-9885-3.